Multifrequency focusing and wide angular scanning of Terajets

V. Pacheco-Peña,[1] M. Beruete,[1,*] I.V. Minin,[2] O. V. Minin,[2]

[1]*Antennas Group - TERALAB, Universidad Pública de Navarra, Campus Arrosadía, 31006 Pamplona, Spain*
[2]*Siberian State Academy of Geodesy, Plahotnogo 10, Novosibirsk, 630108, Russia*
Corresponding author: miguel.beruete@unavarra.es

In the past, it has been demonstrated that it is possible to produce terajets with high resolution at its focus using 3D dielectric cuboids under plane wave illumination. Here, a systematic study of the harmonic and angular response of terajets using cuboids is performed. Mutifrequency focusing is demonstrated at the fundamental frequency and two higher-frequency harmonics showing an intensity enhancement of ~10, ~18 and ~14 for each case. This capability to use 3D dielectric cuboids to produce Terajets at the fundamental frequency and first harmonic is experimentally evaluated at sub-THz frequencies, with good agreement with numerical results. Moreover, a robust angular response is demonstrated numerically and experimentally showing that the intensity at the focal position is maintained in a wide angular range (from 0 to 45 deg); demonstrating the capability to work as a wide scanning terajet focusing lens. The results here presented may be scaled at different frequency bands such as optical frequencies and may be used in microscopy techniques and sensors. © 2014 Optical Society of America

The diffraction of electromagnetic waves [1] has been intensively studied for many years in order to enhance the resolution in microscopy applications. Several techniques have been proposed to solve this problem by improving the design of lenses, such as the application of metamaterials concepts [2], Luneburg lenses [3,4], super oscillation techniques [5,6], novel devices based on spherical dielectric particles [7,8] and diffractive optics [9]. An interesting way to improve resolution beyond the diffraction limit was proposed several years ago using microscaled cylindrical and spherical dielectrics (2D and 3D, respectively), demonstrating the ability to generate subwavelength photonic nanojets with a resolution of $\lambda_0/3$ [10–16], where λ_0 is the operation wavelength. Recently, an alternative mechanism to generate jets at terahertz (THz) and sub-THz frequencies has been proposed and experimentally verified using 3D dielectric cuboids illuminated with a plane wave [17]. It has been demonstrated that, similarly to photonic nanojets with microscaled dielectrics, a refractive index contrast of less than 2:1 between a 3D dielectric cuboid and the background medium should be selected in order to produce terajets just at the output face of the cuboid. It was found that a refractive index $n = 1.41$ is optimal when the cuboid is embedded in vacuum.

In this paper, that study is extended by analyzing the multifrequency focusing properties of the terajets generated by 3D dielectric cuboids at frequency harmonics. First, the multifrequency focusing properties of terajets are numerically evaluated at the fundamental frequency and two frequency harmonics in terms of the focal length (FL), power enhancement and full-width at half-maximum along the transversal x-axis (FWHM$_x$) at each focal length. Simulation results demonstrate that a

terajet appears in all cases, although it is somewhat deteriorated at the second harmonic. The terajet performance at frequency harmonics is experimentally demonstrated at $f_{0exp} = 35$ GHz ($\lambda_{0exp} = 8.57$ mm) and $f_{1exp} = 70$ GHz ($\lambda_{1exp} = 4.28$ mm) for the fundamental frequency and first harmonic, respectively. Experimental results of the power distribution along the transversal x-axis at $z = 0.1\lambda_{0exp}$ for both frequencies are presented and compared with numerical simulations with good agreement between them, demonstrating the capability to use the 3D dielectric cuboids working at frequency harmonics to generate terajets. Moreover, the terajet performance under oblique incidence is studied experimentally and numerically showing that the terajet is deflected at different output angles with a clear dependence with the angle used to illuminate the cuboid. Interestingly, it is revealed that the intensity in the terajet region is preserved for input angles from 0º up to 45º.

All numerical simulations in this letter are performed using the transient solver of the commercial software CST Microwave Studio™, with the same boundary conditions and mesh parameters as [17] and exciting the cuboid with a vertically polarized plane wave (E_y). In the simulation results, both frequency and wavelength will be normalized as $f' = fL/c$ and $\lambda' = \lambda/L$, where primed magnitudes are normalized values and unprimed ones are physical values, L is the dimension of the 3D dielectric cuboid along x and y axes, and c is the velocity of light in vacuum. A 3D dielectric cuboid with thickness $H = 1.2L$ and refractive index $n = 1.41$ embedded in vacuum ($n_0 = 1$) is considered.

To begin with, the harmonic frequency response of terajets is studied. Simulation results of the power distribution in the $yz(E)$ plane and $xz(H)$ plane at the

normalized fundamental frequency ($f_0' = 1$, $\lambda_0' = 1$) and also at the first ($f_1' = 2$, $\lambda_1' = 1/2$) and second ($f_2' = 3$, $\lambda_2' = 1/3$) frequency harmonics are shown in Fig. 1. A terajet is produced in all cases but for the second harmonic ($\lambda_2' = 1/3$) it is slightly deteriorated, with higher side lobes compared with the other cases. By comparing both E and H planes for each frequency in Fig. 1, an interesting feature can be observed: a quasi-symmetric focus is maintained in all cases, demonstrating that it is possible to use the same structure at different harmonics while maintaining its resolution.

In order to better compare this multifrequency terajet performance, simulation results of the normalized power distribution along the optical z-axis are shown in Fig. 2(a), where the power is normalized to the maximum among all cases. From these results, the focal length is FL = -$0.077\lambda_0'$, $0.16\lambda_1'$ (= $0.08\lambda_0'$) and $-0.067\lambda_2'$ (= $0.022\lambda_0'$) for the fundamental frequency and the first and second harmonics, respectively. As it can be observed, the highest intensity is obtained for the first harmonic. Regarding the exploration range Δz (defined as the distance from the output surface at which the intensity has decayed to half its maximum value [17]), the values obtained are Δz = $0.72\lambda_0'$, $0.86\lambda_1'$ (= $0.43\lambda_0'$) and $0.58\lambda_2'$ (= $0.19\lambda_0'$), respectively. As mentioned before, the terajet generated at the second harmonic is slightly deteriorated and a clear

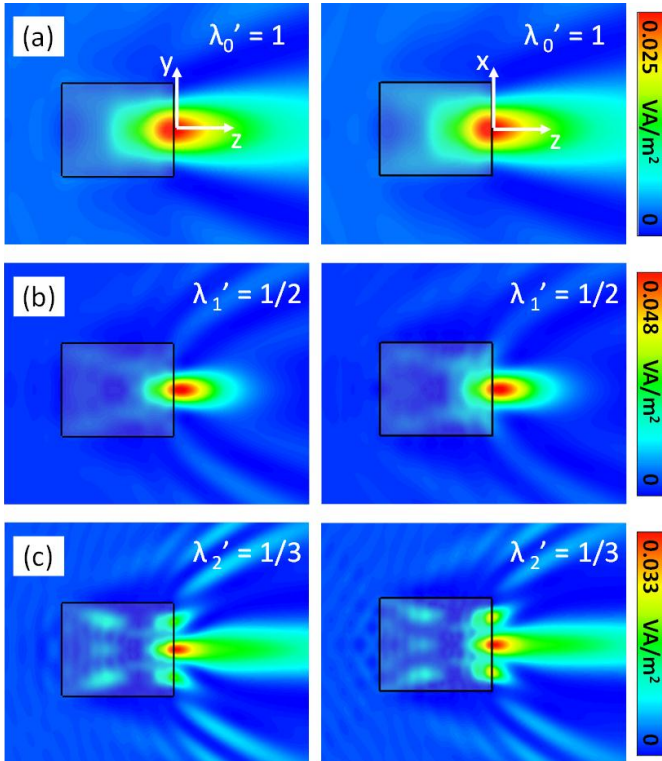Fig. 1. Simulation results of the power distribution in the E-plane (left column) and H-plane (right column) when the 3D dielectric cuboid (with dimensions L along both x- and y- axes and H along z-axis) is illuminated with a plane wave under normal incidence at: (a) the fundamental frequency $\lambda_0' = 1$ and the (b) first $\lambda_1' = 1/2$ and (c) second $\lambda_2' = 1/3$ frequency harmonics.
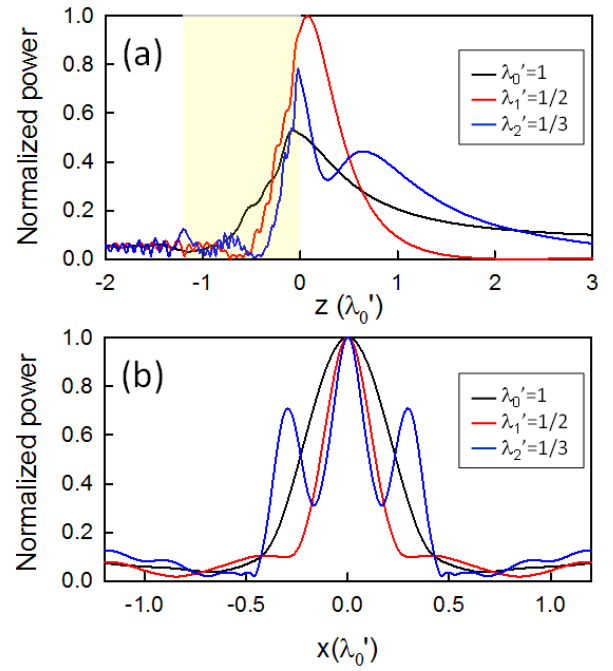

Fig. 2. (a) Simulation results of the normalized power distribution along the z-axis when the 3D dielectric cuboid (yellow block) is evaluated at: the fundamental frequency $\lambda_0' = 1$ (black line), first $\lambda_1' = 1/2$ (red line) and second $\lambda_2' = 1/3$ (blue line) frequency harmonics. The power distribution is normalized with respect to the maximum value obtained among all the frequencies, first harmonic in this case. (b) Simulation results of the normalized power distribution along the transversal x-axis at the numerical focal length for each frequency. In this case, the power distribution is normalized with respect to maximum obtained for each frequency.

secondary peak is observed away from the output surface of the cuboid at $z\sim2.1\lambda_2'$ (=$0.7\lambda_0'$), while the focusing properties of the terajet are not changed for the first harmonic.

Moreover, simulation results of the normalized power distribution along the transversal x-axis just at the output surface of the 3D dielectric cuboid are shown in Fig. 2(b). From these results, the transversal resolution along the x-axis is FWHM$_x$ = $0.47\lambda_0'$, $0.52\lambda_1'$ (= $0.26\lambda_0'$) and $0.62\lambda_2'$ (= $0.21\lambda_0'$), respectively. Also, the power enhancement factor (calculated as the received power at the focal position compared with the power received without the 3D dielectric cuboid) is ~10, ~18 and ~14 at each frequency. Subwavelength resolution is achieved in all frequencies evaluated, but with relatively high side lobes are observed for the second harmonic. These results are summarized in Table I.

The terajet at different frequency harmonics was evaluated experimentally at sub-THz frequencies using the method of movable probe [18]. The experimental frequencies are f_{0exp} = 35 GHz (λ_{0exp} = 8.57 mm) and f_{1exp} = 70 GHz (λ_{1exp} = 4.28 mm) for the fundamental frequency and first harmonic, respectively. A high gain horn antenna was used as source and it was placed at a distance >$2D^2/\lambda_{0exp}$ from the dielectric cuboid in order to illuminate it with a plane wave. A probe was used as a

detector in order to record the power received at a distance of $z = 0.1\lambda_{0exp}$ to the output face of the dielectric cuboid , see a schematic representation of the setup in Fig. 3(a). The cuboid was fabricated with Teflon (n = 1.46) with the dimensions described before: $L = \lambda_{0exp}$ and $H = 1.2\lambda_{0exp}$. Experimental and simulation results of the normalized power distribution along the transversal x-axis at $z = 0.1\lambda_{0exp}$ under normal incidence are shown in Fig. 3(b). A good agreement can be observed, with experimental (numerical) values of $FWHM_x$ $0.46\lambda_{0exp}$ $(0.47\lambda_{0exp})$ and $0.52\lambda_{1exp}$ $(0.53\lambda_{1exp})$ for the fundamental and first frequency harmonic, respectively, demonstrating the capability to use 3D dielectric cuboids at THz and sub-THz frequencies working with frequency harmonics.

Table 1. Simulation results of the terajet performance using the 3D dielectric cuboid with refractive index $n = 1.41$ using plane wave illumination under normal incidence

Frequency	FL[a]	Enhancement	$FWHM_x$[b]	Δ_z[c]
$f_0' = 1$ $(\lambda_0' = 1)$	$-0.077\lambda_0'$	~10	$0.47\lambda_0'$	$0.72\lambda_0'$
$f_1' = 2$ $(\lambda_1' = 1/2)$	$0.16\lambda_1'$	~18	$0.53\lambda_1'$	$0.86\lambda_1'$
$f_2' = 3$ $(\lambda_2' = 1/3)$	$-0.067\lambda_2'$	~14	$0.62\lambda_2'$	$0.58\lambda_2'$

[a]FL is the focal length.

[b]$FWHM_x$ is the full width at half maximum along the x-axis just at the output surface of the 3D dielectric cuboid for each harmonic.
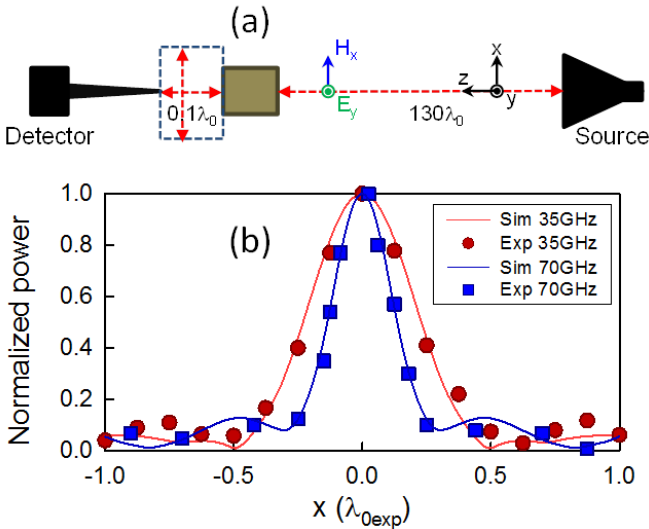
[c]Δ_z is the exploration range.

Fig. 3. (a) Schematic representation on the xz-plane of the experimental setup used to characterize the focusing properties of Terajets. (b) Simulation (continuous lines) and experimental results (symbols) of the normalized power distribution for the fundamental frequency f_{0exp} = 35 GHZ, λ_{0exp} = 8.57 mm (red plots) and first harmonic f_{1exp} = 70 GHZ, λ_{1exp} = 4.28 mm (blue plots) at $z = 0.1\lambda_{0exp}$
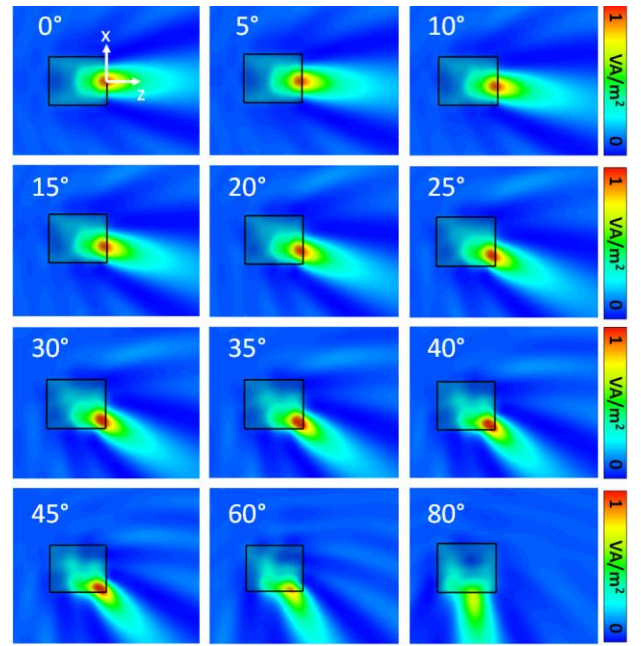

Fig. 4. Simulation results of the normalized power distribution in the $xz(H)$ plane for the 3D dielectric cuboid under oblique incidence at the fundamental frequency (λ' = 1) for the input angles 0º, 5º, 10º, 15º, 20º, 25º, 30º, 35º, 40º, 45º, 60º and 80º. Simulation results are normalized with respect to the maximum power obtained under normal illumination (0º).

It is also important to evaluate the focusing properties under oblique incidence, to characterize the robustness of terajets at different angles. Simulation results of the normalized power distribution in the $xz(H)$ plane for input angles from 0° to 80° are shown in Fig. 4 particularized only for the fundamental frequency, f' = 1. It can be observed that the terajet is deflected when the input angle is changed, as expected.

The experiments were carried out at 100GHz (λ_0=3mm) by using a 3D dielectric cuboid fabricated with the same normalized dimensions used through this letter to work at this wavelength. The experimental setup along with the pictures of the probe used as a detector, the 3D dielectric cuboid and the horn antenna used as source are shown in Fig. 5(a-d). The cuboid was placed in a screen surrounded with absorbers in order to avoid undesirable reflections. The source was placed at the distance ~130λ_0 from the back face of the cuboid and it was rotated at the needed input angle in order to illuminate the structure with a plane wave under oblique incidence. In order to record the received power, the detector was fixed at the same input angle and a 2D scanning on the $x'z'$-plane was performed with the aim to obtain the exact position of the maximum intensity. Finally, the output angle was corrected based on this position.

Based on this, and in order to better compare the results of plane wave illumination under oblique incidence, simulation results of the output beam deviation versus the input angle are shown in Fig. 5(e) as a continuous line along with experimental results (red symbols) with a good agreement between them. Note that, for the experimental case, the oblique incidence is
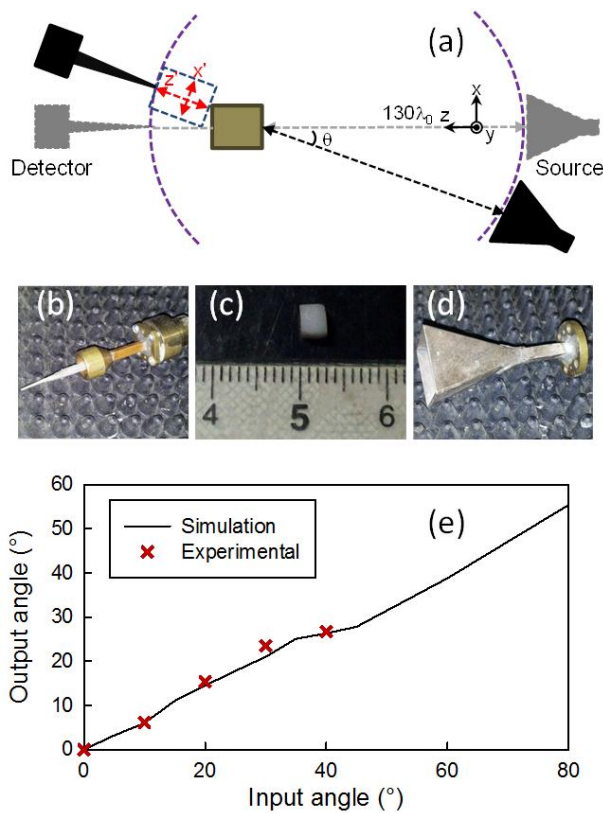
Fig. 5. (a) Schematic representation on the *xz*-plane of the experimental setup used to characterize the focusing properties of Terajets under oblique incidence. (b) Probe used as a detector in the experiment (c) picture of the 3D dielectric cuboid made of teflon and (d) horn antenna used as source. (e) Simulation (continuous line) and experimental results of the output angle of the terajet versus the input angle of the incident plane wave evaluating the 3D dielectric cuboid under oblique incidence for input angles from 0º - 80º and from 0º - 40º for simulation and experiment, respectively.

evaluated for angles up to 40º due to experimental limitations. It is shown from Fig. 5(e) that the beam deviation factor (output angle/input angle) has an almost constant slope with a value of 1 for input angles from 0° to 45°; moreover, the intensity of the terajet at the output face of the 3D cuboid is not reduced for these angles, contrarily to the behavior at 60° and 80°. For the case of the first and second frequency harmonics (not shown here) the same dependences are obtained, demonstrating that the terajet produced by the cuboid has a robust performance even under oblique incidence with relatively high incidence angles.

In conclusion, the capability to generate multifrequency terajets using 3D dielectric cuboids working at frequency harmonics has been studied at THz frequencies. It has been shown that an intensity enhancement of ~10, ~18 and ~14 for the fundamental frequency and the first and second harmonics, respectively, is achieved with a subwavelength focus in all these cases. Also, the terajet performance has been evaluated when the 3D dielectric cuboid is excited by a plane wave under oblique incidence, demonstrating that the terajet is deflected for different

input angles without deterioration in the intensity of the focus for input angles from 0º to 45º; demonstrating the capability to be used as a wide scanning terajet focusing lens. Experimental results of the terajet generated by a 3D dielectric cuboid made of Teflon (n = 1.46) have been presented at sub-THz frequencies with a good agreement with numerical simulations. The results here presented may be scaled to other frequency bands such as optical frequencies and may be applied to enhance the radiation performance of antennas, novel microscopy techniques and sensors.

References.

1. M. Born and E. Wolf, Principles Of Optics, 7th ed. (Cambridge University Press, New York, 1999).
2. T. Roy, E.T.F. Rogers, and N.I. Zheludev, Opt. Express **21**, 7577 (2013).
3. A. Demetriadou and Y. Hao, Opt. Express **19**, 19925 (2011).
4. A. Demetriadou and Y. Hao, IEEE Antennas Wirel. Propag. Lett. **10**, 1590 (2011).
5. E.T.F. Rogers, J. Lindberg, T. Roy, S. Savo, J.E. Chad, M.R. Dennis, and N.I. Zheludev, Nat. Mater. 11, 432 (2012).
6. T. Liu, J. Liu, H. Zhang, and J. Tan, Opt. Commun. **319**, 31 (2014).
7. Y.F. Lu, L. Zhang, W.D. Song, Y.W. Zheng, and B.S. Luk'yanchuk, J. Exp. Theor. Phys. Lett. **72**, 457 (2000).
8. Z. Wang, W. Guo, L. Li, B. Luk'yanchuk, A. Khan, Z. Liu, Z. Chen, and M. Hong, Nat. Commun. **2**, 218 (2011).
9. O. V. Minin and I. V. Minin, in Class. Opt. 2014 (Osa, Washington, D.C., 2014)
10. Z. Chen, A. Taflove, and V. Backman, Opt. Express **12**, 1214 (2004).
11. S. Lecler, Y. Takakura, and P. Meyrueis, Opt. Lett. **30**, 2641 (2005).
12. X. Li, Z. Chen, A. Taflove, and V. Backman, Opt. Express **13**, 526 (2005).
13. A. Heifetz, S.-C. Kong, A. V Sahakian, A. Taflove, and V. Backman, J. Comput. Theor. Nanosci. **6**, 1979 (2009).
14. A. Heifetz, K. Huang, A. V. Sahakian, X. Li, A. Taflove, and V. Backman, Appl. Phys. Lett. **89**, 221118 (2006).
15. C. Liu, Prog. Electromagn. Res. Lett. 37, 153 (2013).
16. D. Ju, H. Pei, Y. Jiang, and X. Sun, Appl. Phys. Lett. **102**, 171109 (2013).
17. V. Pacheco-Peña, M. Beruete, I. V. Minin, and O. V. Minin, Appl. Phys. Lett. **105**, 084102 (2014).
18. I. V. Minin and O. V. Minin, Chinese Opt. Lett. **12**, 060014 (2014).

(Full References)

1. M. Born and E. Wolf, *Principles Of Optics*, 7th ed. (Cambridge University Press, 1999).
2. T. Roy, E. T. F. Rogers, and N. I. Zheludev, "Sub-wavelength focusing meta-lens.," Opt. Express **21**, 7577–82 (2013).
3. A. Demetriadou and Y. Hao, "Slim Luneburg lens for antenna applications," Opt. Express **19**, 19925–19934 (2011).
4. A. Demetriadou and Y. Hao, "A Grounded Slim Luneburg Lens Antenna Based on Transformation Electromagnetics," IEEE Antennas Wirel. Propag. Lett. **10**, 1590–1593 (2011).
5. E. T. F. Rogers, J. Lindberg, T. Roy, S. Savo, J. E. Chad, M. R. Dennis, and N. I. Zheludev, "A super-oscillatory lens optical microscope for subwavelength imaging.," Nat. Mater. **11**, 432–5 (2012).
6. T. Liu, J. Liu, H. Zhang, and J. Tan, "Efficient optimization of super-oscillatory lens and transfer function analysis in confocal scanning microscopy," Opt. Commun. **319**, 31–35 (2014).
7. Y. F. Lu, L. Zhang, W. D. Song, Y. W. Zheng, and B. S. Luk'yanchuk, "Laser writing of a subwavelength structure on silicon (100) surfaces with particle-enhanced optical irradiation," J. Exp. Theor. Phys. Lett. **72**, 457–459 (2000).
8. Z. Wang, W. Guo, L. Li, B. Luk'yanchuk, A. Khan, Z. Liu, Z. Chen, and M. Hong, "Optical virtual imaging at 50 nm lateral resolution with a white-light nanoscope.," Nat. Commun. **2**, 218 (2011).
9. O. V. Minin and I. V. Minin, "Design of Subwavelength Resolution 3D Diffractive Optics," in *Classical Optics 2014* (Osa, 2014), Vol. 1, p. 2.
10. Z. Chen, A. Taflove, and V. Backman, "Photonic nanojet enhancement of backscattering of light by nanoparticles: a potential novel visible-light ultramicroscopy technique.," Opt. Express **12**, 1214–20 (2004).
11. S. Lecler, Y. Takakura, and P. Meyrueis, "Properties of a three-dimensional photonic jet.," Opt. Lett. **30**, 2641–3 (2005).
12. X. Li, Z. Chen, A. Taflove, and V. Backman, "Optical analysis of nanoparticles via enhanced backscattering facilitated by 3-D photonic nanojets.," Opt. Express **13**, 526–33 (2005).
13. A. Heifetz, S.-C. Kong, A. V Sahakian, A. Taflove, and V. Backman, "Photonic Nanojets.," J. Comput. Theor. Nanosci. **6**, 1979–1992 (2009).
14. A. Heifetz, K. Huang, A. V. Sahakian, X. Li, A. Taflove, and V. Backman, "Experimental confirmation of backscattering enhancement induced by a photonic jet," Appl. Phys. Lett. **89**, 221118 (2006).
15. C. Liu, "Ultra-elongayed photonic nanojets generated by a graded-index microellipsoid," Prog. Electromagn. Res. Lett. **37**, 153–165 (2013).
16. D. Ju, H. Pei, Y. Jiang, and X. Sun, "Controllable and enhanced nanojet effects excited by surface plasmon polariton," Appl. Phys. Lett. **102**, 171109 (2013).
17. V. Pacheco-Peña, M. Beruete, I. V. Minin, and O. V. Minin, "Terajets produced by dielectric cuboids," Appl. Phys. Lett. **105**, 084102 (2014).
18. I. V. Minin and O. V. Minin, "3D diffractive lenses to overcome the 3D Abbe subwavelength diffraction limit," Chinese Opt. Lett. **12**, 060014–1–3 (2014).